Possible antiferroquadrupolar order in the Kondo semiconductor CeOs$_4$Sb$_{12}$

Takashi Tayama,[*] Yusuke Kani, Momota Imai, and Yuta Kanai

Graduate School of Science and Engineering, University of Toyama, Toyama 930-8555, Japan

Hitoshi Sugawara

Department of Physics, Kobe University, Kobe 657-8501, Japan

We report the results of dc magnetization, thermal expansion, and magnetostriction measurements of the Kondo semiconductor CeOs$_4$Sb$_{12}$. These results provide a magnetic-field–temperature phase diagram for the three principal axes of the cubic crystal [100], [110], and [111] and reveal the magnetic anisotropy of the three ordered phases A, B, and C. The magnetic anisotropy of the transition temperature T_C from the paramagnetic phase to the C phase is $T_C^{[111]} > T_C^{[110]} > T_C^{[100]}$. At low temperatures, the magnetization has a distinct magnetic anisotropy in high magnetic fields: $M^{[100]} > M^{[110]} > M^{[111]}$. This ratio of magnetization is in good agreement with that of the magnetically anisotropic Γ_{67} quartet. The observation indicates that the crystalline electric field ground state is a Γ_{67} quartet and that the c-f hybridization effect is nearly isotropic. In addition, comparison of the present experimental results with numerical calculations of a two-sublattice model using the mean-field approximation suggests that the C phase is a Γ_5-type antiferroquadrupolar ordered state despite the presence of strong c-f hybridization effects. In this case, the increase in T_C due to the external field is mainly caused by the Γ_2-type antiferro-octupolar interaction.

I. INTRODUCTION

The Ce-based filled skutterudite CeT$_4$X$_{12}$ (T = Fe, Ru, or Os; X = P, As, or Sb) crystallizes in a cubic LaFe$_4$P$_{12}$-type structure (space group $Im\bar{3}$). The electrical conductivity of Ce-based filled skutterudites can be roughly classified according to their lattice constants: CeT$_4$X$_{12}$ with X = P and As is a Kondo semiconductor, while CeT$_4$X$_{12}$ with X = Sb, which has a larger lattice constant than those, is a metal. However, CeOs$_4$Sb$_{12}$ is an exception: Despite having the largest lattice constant among the Ce-filled skutterudites, it is a Kondo semiconductor; its energy band gap is very small, $\Delta E/k_B \approx 10$ K [1,2]. According to the band structure calculation, CeOs$_4$Sb$_{12}$ has a Fermi surface nesting structure [3–5]. The main conduction band consists of the p orbitals of the pnictogen surrounding the Ce ions, which are strongly hybridized with the 4f electron. This c-f hybridization effect results in a hybridization-induced band gap at low temperatures, making it a Kondo semiconductor [2,3,6]. When an external magnetic field H is applied, the electrical conductivity changes from semiconducting to metallic behavior [7]. In fact, the Fermi surface in high magnetic fields has been observed by experiments on the de Haas–van Alphen and Shubnikov–de Haas oscillations [8].

An interesting feature of this material is the presence of three ordered phases A, B, and C at low temperatures (Fig. 1, top panel) [7,9–13]. In zero field, the A and B phase transitions occur at $T_A = 1.1$ K and $T_B = 0.8$ K, respectively, and the

A phase transition is attributed to antiferromagnetic (AFM) ordering. According to neutron scattering experiments, the propagation vector of the AFM structure is $q = (100)$, and the magnitude of the order moment is as small as 0.07 μ_B/Ce [14–16]. This AFM order also exists in the B phase and is interpreted to be due to the spin density wave (SDW) transition caused by Fermi surface nesting with $q = (100)$. However, this material is a Kondo semiconductor at zero field and has no Fermi surface. Therefore it is not clear whether such a SDW transition can occur.

The application of a magnetic field of 1 T suppresses the AFM order and induces a transition to the C phase with a ferromagnetic component [11,12]. Interestingly, the transition temperature T_C from the paramagnetic phase to the C phase increases significantly with increasing magnetic field, and the C phase has a field-induced reentrant phase boundary [7]. A theoretical model of SDW order due to band nesting with $q = (100)$ has also been proposed for the C phase [4,5], and the increase in T_C with the magnetic field is explained by the improvement of the Fermi surface nesting condition by the external field. This model predicts that a staggered magnetic moment is induced in the direction perpendicular to the magnetic field, but no such moment has been observed in neutron scattering experiments when the magnetic field is applied along the [100] direction [16]. Also, in this model, the increase in T_C is at most 1.5 times, which is quite smaller than the experimental value. Therefore the order parameter of phase C remains unresolved.

On the other hand, the value of entropy at zero field is remarkably small (the entropy change below T_A is roughly 0.05R ln 2 J/mol K) [17]. In addition, no crystalline electric
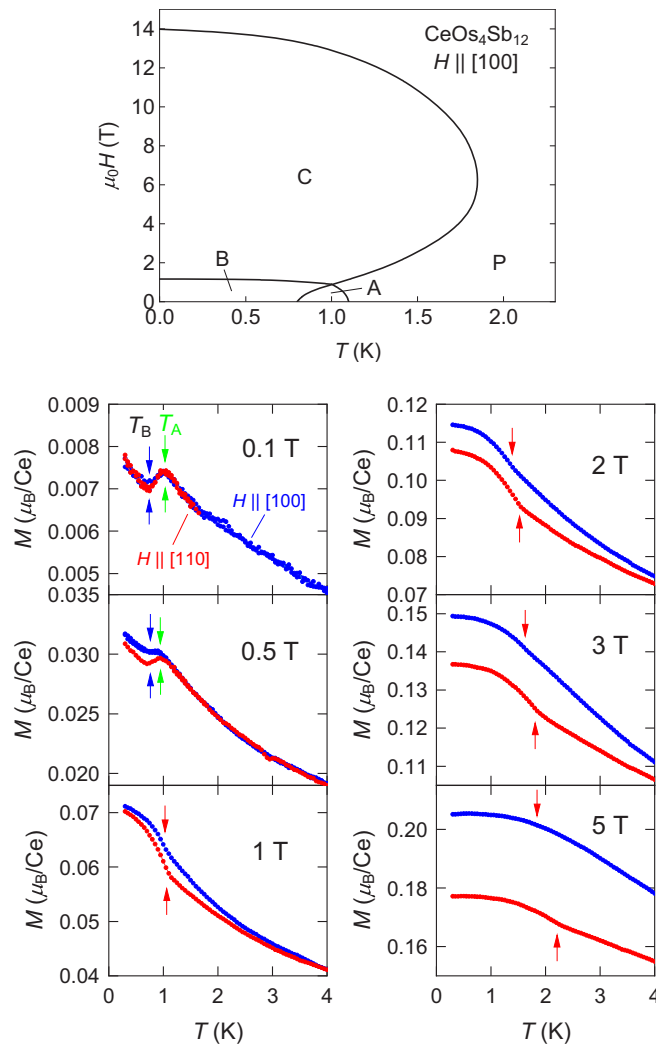
*tayama@sci.u-toyama.ac.jp

FIG. 1. Top panel: Overview of the magnetic phase diagram of CeOs$_4$Sb$_{12}$ for $H \parallel$ [100] reported so far. The data below and above 5 T were taken from Refs. [13] and [7], respectively. P denotes the paramagnetic phase, and A, B, and C denote the ordered phase (see text for details). Bottom panels: Temperature dependence of the dc magnetization $M(T)$ below 4 K in CeOs$_4$Sb$_{12}$ when a magnetic field H is applied along the [100] (blue dots) and [110] (red dots) directions, respectively. From top left to bottom right, the results at $\mu_0 H = 0.1$, 0.5, 1, 2, 3, and 5 T, respectively. The green, blue, and red arrows indicate the transition temperatures of T_A, T_B, and T_C, respectively.

field (CEF) excited states have yet been observed in inelastic neutron scattering experiments [14]. These results demonstrate that the localized picture of $4f$ electron is not effective in this material. Nevertheless, the information on the CEF energy levels is very important as a starting point to elucidate the ordered states. The crystal symmetry of the Ce site belongs to the cubic point group T_h (but is effectively equal to O_h for a Ce^{3+} ion). Due to this cubic T_h symmetry CEF effect, the $J = 5/2$ ground-state multiplet in the $4f$ electron of Ce^{3+} splits into a Γ_5 doublet and a Γ_{67} quartet. Analysis of the magnetic susceptibility of polycrystalline samples suggests that the CEF ground state is the Γ_5 doublet [1]. However, it is difficult to extract multiple ordered phases with different

properties from the Γ_5 doublet alone, which has only magnetic degrees of freedom. Therefore the CEF ground state is still a matter of debate.

In this paper, dc magnetization, thermal expansion, and magnetostriction measurements on a single-crystal sample of CeOs$_4$Sb$_{12}$ are performed to investigate the magnetic anisotropy in both the magnetic phase diagram and the CEF ground state. The magnetization at low temperatures shows a distinct magnetic anisotropy: $M^{[100]} > M^{[1\bar{1}0]} > M^{[111]}$. Interestingly, the ratio of this magnetic anisotropy is exactly the same as that of the Γ_{67} quartet. The observation strongly suggests that the CEF ground state is the Γ_{67} quartet, not the Γ_5 doublet as previously reported. In spite of the strong c-f hybridization effect, the magnetic anisotropy of the Γ_{67} quartet is maintained, suggesting that the c-f hybridization effect is almost isotropic. The magnetic field angle dependence of $T_C(\theta)$ within the (001) and (1$\bar{1}$0) planes at 5 T shows a smooth variation, and the T_C for the three principal axes is $T_C^{[111]} > T_C^{[110]} > T_C^{[100]}$. Comparing the present experimental results with numerical calculations using a two-sublattice model that incorporate quadrupolar and octupolar interactions in the mean-field approximation, we find that the C phase is likely to be a Γ_5-type antiferroquadrupolar (AFQ) order. The significant increase in T_Q with the application of a magnetic field can be understood mainly by a Γ_2-type antiferro-octupolar interaction.

II. EXPERIMENT

Single-crystal samples of CeOs$_4$Sb$_{12}$ were prepared by the self-flux method using Sb. The details of the single-crystal samples are described in Ref. [7]. The single-crystal sample used in this experiment has a mass of 1.83 mg and a shape similar to a cube. The length of the sample along the [100] direction is $L_{100} = 0.76$ mm and along the [110] direction is $L_{110} = 0.64$ mm.

The dc magnetization measurements in the temperature (T) range from 0.25 to 4 K were performed using the capacitance Faraday method. The capacitive magnetometer has a sensitivity of $\sim 10^{-6}$-10^{-5} emu. The measurements were performed using a magnetic field gradient of 8 T/m. We also used a Quantum Design superconducting quantum interference device (SQUID) magnetometer for dc magnetization measurements in the temperature range from 2 to 300 K. Linear thermal expansion and linear magnetostriction measurements were performed using the capacitance method. The capacitive dilatometer used in this study allows us to measure samples of any shape and has a measurement sensitivity of 0.01–0.1 Å.

For both dc magnetization and thermal expansion measurements, the sample was mounted in a ^{3}He refrigerator, and capacitance was read using a high-sensitivity capacitance bridge (Andeen-Hargerling, model 2500A). The longitudinal ($H \parallel L$) and transverse ($H \perp L$) magnetostrictions with respect to the magnetic field direction were measured using a solenoidal superconducting magnet and a split-pair superconducting magnet, respectively. The field angle dependence of the transverse magnetostriction was measured by rotating a ^{3}He refrigerator with a stepper motor rotator against a split-pair superconducting magnet. The magnetic field range of
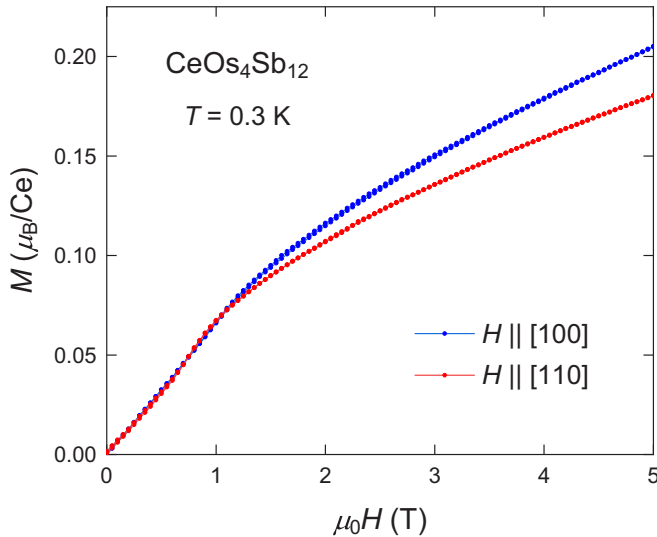
FIG. 2. Isothermal dc magnetization $M(H)$ processes of $CeOs_4Sb_{12}$ at 0.3 K when the magnetic field is applied along the [100] direction (blue dots) and the [110] direction (red dots), respectively. Both sets of data were taken by increasing and then decreasing the magnetic field.

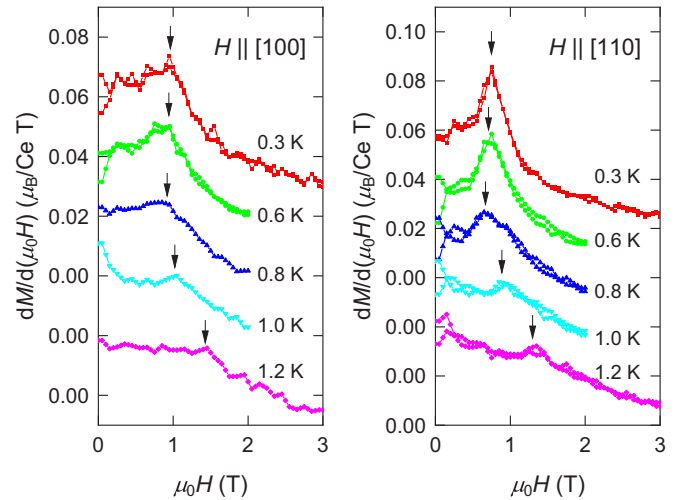FIG. 3. Magnetic field dependence of the differential magnetic susceptibility $dM(H)/dH$ of $CeOs_4Sb_{12}$ at temperatures below 1.2 K. Left and right panels are results for $H \parallel [100]$ and $H \parallel [110]$, respectively. Arrows indicate the transition field to the C phase. Note that the origin of each set of data is shifted.

the measurement is from 0 to 5 T. Note that some of the dc magnetization and thermal expansion results for $H \parallel [100]$ shown here have already been published in Ref. [13].

III. RESULTS

A. dc magnetization

The bottom panels of Fig. 1 show the temperature dependence of the magnetization $M(T)$ below 4 K in $CeOs_4Sb_{12}$ when the magnetic field is applied along the [100] and [110] directions, respectively. The data at 0.1 T for the [100] direction show a peak at $T_A = 1.1$ K. This is due to the AFM transition. As the temperature is further decreased, the $M(T)$ curve bends upward at $T_B = 0.8$ K, and the magnetization continues to increase up to our lowest temperature of measurement. The results for the [100] and [110] directions are almost identical, indicating that the magnetization is isotropic. Since the magnetization is generally anisotropic in the magnetically ordered state, the observed isotropy of magnetization suggests the formation of magnetic domains below the T_A. Note that no temperature hysteresis is observed within the experimental error.

The results at 0.5 T also show anomalies at T_A and T_B, but below T_A, weak magnetic anisotropy is observed. This can be understood as an evolution to a single magnetic domain. At fields above 1 T, there is no peak due to the A phase transition, but an upward bending similar to the T_B anomaly at zero field. As previously reported, this anomaly is due to a transition to the C phase [13]. The transition temperature T_C increases with increasing magnetic field up to our maximum field of 5 T in both directions. The anomaly in T_C for $H \parallel [100]$ is not clear, so the T_C shown here is obtained from the results of thermal expansion, as will be explained later. Figure 2 shows the isothermal magnetization $M(H)$ process of $CeOs_4Sb_{12}$ at 0.3 K when the magnetic field is applied along the [100]

and [110] directions, respectively. The data were taken by increasing the magnetic field up to 5 T and then decreasing the magnetic field. The $M(H)$ curve is nearly linear and isotropic up to around 1.2 T, but shows magnetic anisotropy at higher fields. There is no apparent magnetic hysteresis in these data. To examine the $M(H)$ data in more detail, the resulting differential magnetic susceptibility $dM(H)/dH$ is shown in Fig. 3. The data at 0.3 K for the [100] and [110] directions show peaks at 1 and 0.8 T, respectively. Here, we define the peak as the transition field, H_C, to the C phase. As the temperature is increased, the H_C does not change much up to about 1 K, but gradually shifts to higher fields above 1 K.

Figure 4 shows the $M(H)$ curves at 2 K when the magnetic field is applied along each of the three principal axes.
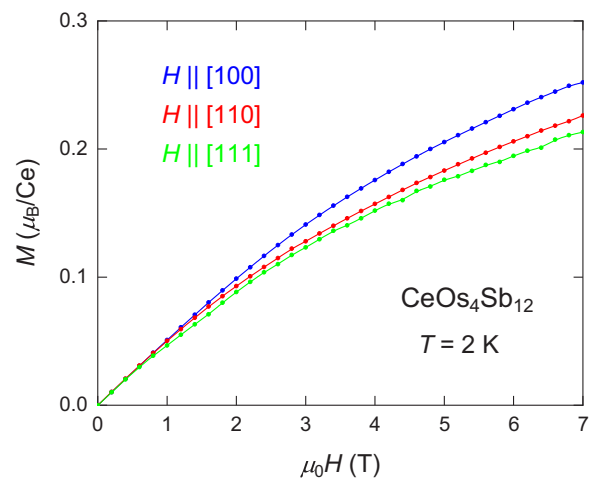

FIG. 4. Isothermal magnetization $M(H)$ process of $CeOs_4Sb_{12}$ at 2 K when a magnetic field is applied along the three principal axes of the cubic crystal, [100], [110], and [111], respectively. The data were collected by increasing the magnetic field to 7 T.
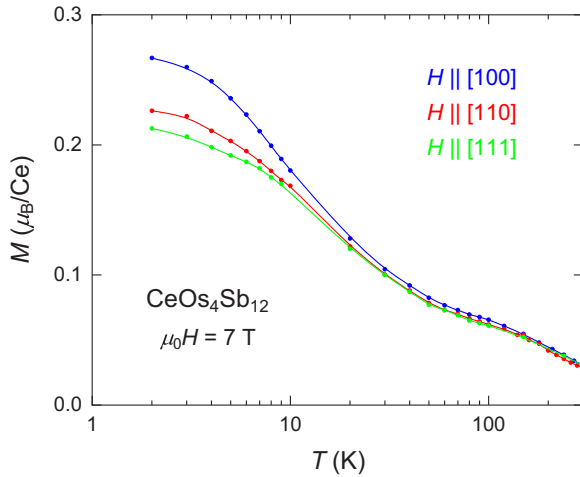
FIG. 5. Temperature dependence of the magnetization $M(T)$ in CeOs$_4$Sb$_{12}$ when a magnetic field of 7 T is applied along the three principal axes of the cubic crystal, [100], [110], and [111], respectively. Note that the horizontal axis of the figure is a logarithmic scale.

In all three directions, the magnetization increases smoothly with the magnetic field. An important feature of this result is a distinct magnetic anisotropy of $M^{[100]} > M^{[110]} > M^{[111]}$. Taking the ratio of the magnitudes of the magnetization in the three directions at 7 T, we get $M^{[100]} : M^{[110]} : M^{[111]} = 1.2 : 1.08 : 1$. As will be shown later in the thermal expansion results, there is a transition to the C phase near 4 T in the 2-K data for the [110] and [111] directions. However, since there is no obvious anomaly near 4 T in the $M(H)$ curve at 2 K, the anisotropy ratio of the magnetization obtained here would be almost the same as that of the paramagnetic state. The magnetization ratio will be discussed later.

Figure 5 shows the temperature dependence of the magnetization $M(T)$ in CeOs$_4$Sb$_{12}$ when a magnetic field of 7 T is applied along the [100], [110], and [111] directions, respectively. As the temperature is decreased from 300 K, the $M(T)$ curve increases monotonically, and the magnetic anisotropy develops gradually. In addition, the results show a small hump around 100 K and a saturation trend below 10 K.

B. Thermal expansion and magnetostriction

Figure 6 shows the temperature dependence of the longitudinal ($H \parallel L$) linear thermal expansion $\Delta L(T)/L$ for $H \parallel$ [100] and $H \parallel$ [110] of CeOs$_4$Sb$_{12}$ at several fixed magnetic fields up to 5 T. In the paramagnetic state, the $\Delta L(T)/L$ data at zero field decrease linearly with temperature, and the results for $H \parallel$ [100] and $H \parallel$ [110] are nearly the same. This is to be expected from the cubic structure. Both data for $H \parallel$ [100] and data for $H \parallel$ [110] show a peak due to the AFM transition at $T_A = 1.1$ K. As the temperature is lowered further, the B phase transition appears at $T_B = 0.8$ K. Below this temperature, the results for $H \parallel$ [100] and $H \parallel$ [110] are apparently different. This indicates that the cubic symmetry is nearly preserved in the A phase while it is reduced from cubic symmetry in the B phase. This contrasts with the fact that the magnetization is isotropic even below T_B (see Fig. 1).
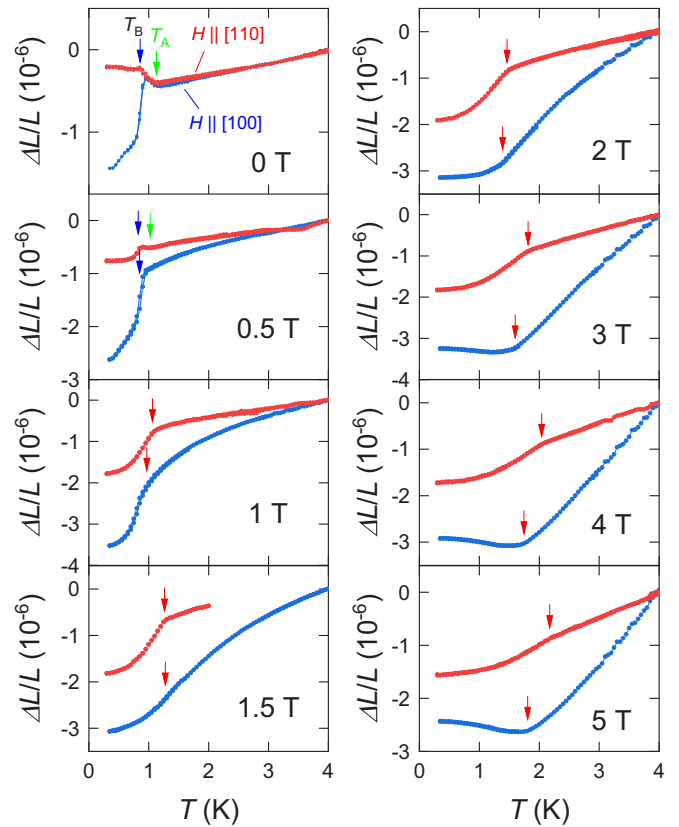

FIG. 6. Temperature dependence of the longitudinal ($H \parallel L$) linear thermal expansion $\Delta L(T)/L$ of CeOs$_4$Sb$_{12}$ for $H \parallel$ [100] (blue dots) and $H \parallel$ [110] (red dots). Each set of data was taken by increasing and then decreasing the temperature. The arrows indicate the transition from phase A to phase B. The value of $\Delta L(T)/L$ is shifted so that it becomes zero at 4 K. The green, blue, and red arrows indicate the transition temperatures of T_A, T_B, and T_C, respectively.

In the data at 0.5 T, the results in the [100] and [110] directions are slightly different even in the paramagnetic state, indicating magnetic anisotropy. Compared with the T_B anomaly, the T_A anomaly is less obvious in the data for both directions. At fields above 1 T, there is only one anomaly due to the transition from the paramagnetic phase to the C phase, as seen in the magnetization results. Also, the result for $H \parallel$ [100] bends upward at T_C, while the result for $H \parallel$ [110] bends downward at T_C. It turns out that the anomaly at T_C in the thermal expansion is more obvious than the anomaly in the magnetization. Figure 7 shows the magnetic field dependence of the longitudinal linear magnetostriction $\Delta L(H)/L$ for $H \parallel$ [100] and $H \parallel$ [110] at 0.3 K in CeOs$_4$Sb$_{12}$. The data for $H \parallel$ [100] and $H \parallel$ [110] show anomalies due to the phase transition at around 1.1 and 1.2 T, respectively. Compared with the results for $H \parallel$ [100], the $\Delta L(H)/L$ curve for $H \parallel$ [110] does not change much above H_C. To confirm these results in more detail, the longitudinal magnetostriction coefficient $\lambda = \frac{d}{dH}(\frac{\Delta L(H)}{L})$ is shown in Fig. 8. The data at 0.3 K for $H \parallel$ [100] (left panel) show a rather sharp peak at 1.1 T. This is due to the transition from phase B to phase C. In addition, there is an anomaly around 0.2 T. On the other hand, the data for $H \parallel$ [110] at 0.3 K (right panel) also show two peaks at
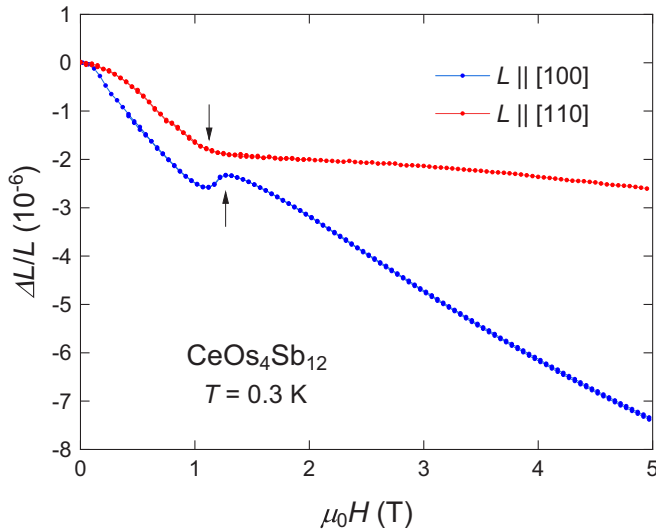
FIG. 7. Magnetic field dependence of the longitudinal ($H \parallel L$) linear magnetostriction $\Delta L(H)/L$ of $CeOs_4Sb_{12}$ when a magnetic field is applied along the [100] and [110] directions, respectively. Arrows indicate the transition field to the C phase. The origin of each set of data is shifted so that it becomes zero.

0.6 and 1 T. The anomaly at 1.1 T is presumably due to the transition to C phase. The data at 0.7 K are similar to the data at 0.3 K, but only one anomaly is seen at 1.0 K. As the temperature is further increased, the peak gradually shifts to higher fields. Figure 9 shows the results of the transverse linear thermal expansion at various fixed magnetic fields when the magnetic field is applied along the [111] direction. The data at zero field show anomalies at $T_A = 1.1$ K and $T_B = 0.8$ K, and the data at 0.5 T are similar to the data at zero field. In the data above 1 T, the anomalies at T_C are more pronounced
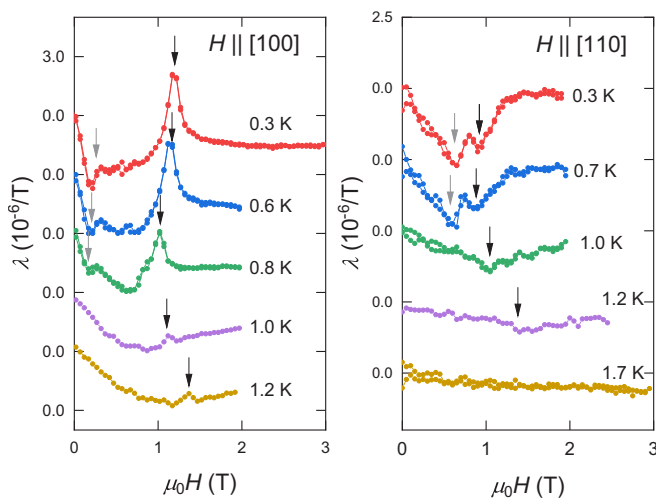

FIG. 9. Temperature dependence of the transverse ($H \perp L$) linear thermal expansion of $CeOs_4Sb_{12}$ when a magnetic field is applied along the [111] direction. The green, blue, and red arrows indicate the transition temperatures of T_A, T_B, and T_C, respectively. Note that the origin of each set of data is shifted.

than those in other magnetic field directions (see Fig. 6). The H-T phase diagram of $CeOs_4Sb_{12}$ obtained from the present thermal expansion and from magnetostriction measurements is shown in Fig. 10. This phase diagram is divided into four phases: the paramagnetic phase P and the three ordered phases A, B, and C. The A and B phases are accompanied by AFM order. The transition temperature T_C from the paramagnetic phase to the C phase is lowest in the [100] direction and highest in the [111] direction; that is, $T_C^{[111]} > T_C^{[110]} > T_C^{[100]}$. The T_C for the [110] or [111] direction at 5 T increases to more than twice the value at zero field ($T_B = 0.8$ K). Phases A and B have a larger area for $H \parallel$ [100] than for $H \parallel$ [110]. Unfortunately, the phase boundary of phases B and C for $H \parallel$ [111] has not yet been obtained. The dashed lines in phase B of $H \parallel$ [100] and $H \parallel$ [110] show the anomalies seen in the magnetostriction. This may be related to changes in magnetic domains.

C. Magnetic field angle dependence of transverse linear magnetostriction

To investigate the magnetic field angle dependence of T_C in more detail, the temperature dependence of the transverse linear thermal expansion $\Delta L(T)/L$ when a magnetic field of 5 T is applied within the (001) plane is shown in Fig. 11. The angle between the [100] direction and the direction of the magnetic field is defined as θ; $\theta = 0°$, 45°, and 90° correspond

FIG. 8. Magnetic field dependence of the longitudinal ($H \parallel L$) linear magnetostriction coefficient in $CeOs_4Sb_{12}$. Left and right panels are results for $H \parallel$ [100] and $H \parallel$ [110], respectively. The black arrows indicate a phase transition to phase C. The gray arrows indicate anomalies within phase B. Note that the origin of each set of data is shifted.
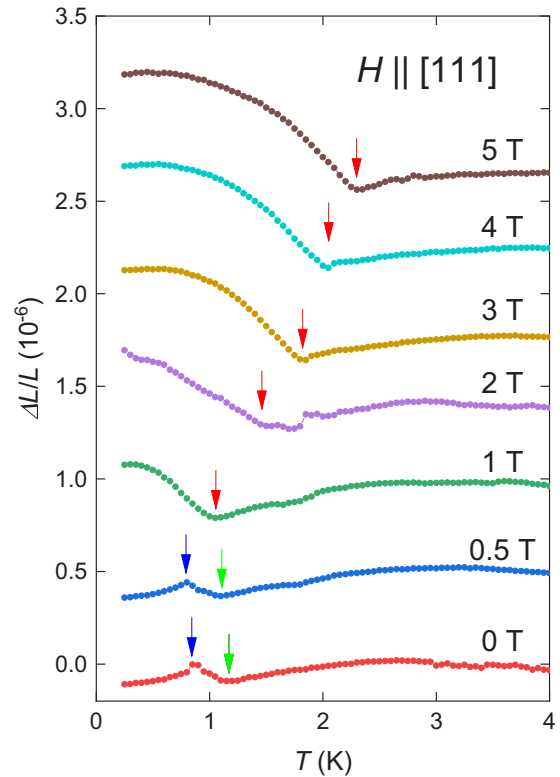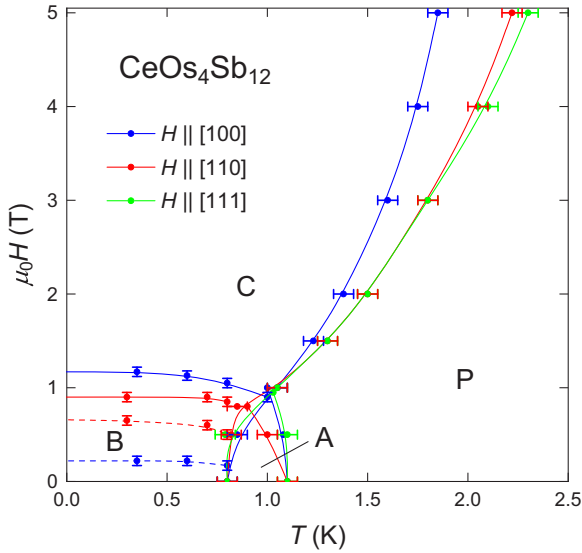
FIG. 10. *H-T* phase diagram for the cubic principal axes [100], [110], and [111] directions in CeOs$_4$Sb$_{12}$ obtained from the present thermal expansion and from magnetostriction measurements. P, paramagnetic phase; A, AFM phase; B and C, B and C phases, respectively. The solid lines and dashed lines are guides for the eye. The solid lines indicate phase boundaries, and the dashed lines indicate anomalies within a phase.

FIG. 11. Temperature dependence of the transverse ($H \perp L$) linear thermal expansion $\Delta L(T)/L$ of CeOs$_4$Sb$_{12}$ when a magnetic field of 5 T is applied within the (001) plane. The magnetic field angle θ is the angle between the magnetic field direction H and the [100] direction within the (001) plane. In other words, $\theta = 0°$, 45°, and 90° correspond to the [100], [110], and [010] directions, respectively. The arrows indicate the transition temperature T_C, and the two dashed lines are guides for the eye, corresponding to the maximum and minimum T_C temperatures. Note that the origin of each set of data is shifted so that the data do not overlap.

to the [100], [110], and [010] directions, respectively. The measurements were taken every 15° between $\theta = -110°$ and $\theta = 70°$. Some of the results are shown in the figure. The transition temperature T_C at each angle is indicated by an arrow. The resulting magnetic field angle dependence of $T_C(\theta)$ in the angle range of $\theta = -120°$ to $+90°$ is shown in Fig. 12. It can be seen that the value of T_C is lowest in the [100] direction and highest in the [110] direction. Since $T_C(\theta)$ shows periodic oscillations, it can be fitted with a single sine function (solid line). The period of the oscillation is 90°, which is consistent with the result expected within the (001) plane with fourfold symmetry. Similarly, the $\Delta L(T)/L$ data when a 5 T magnetic field is applied within the (1$\bar{1}$0) plane are shown in Fig. 13, where $\theta = 0°$, 54.7°, and 90° correspond to the [001], [111], and [110] directions, respectively. The value of T_C is maximum in the [111] direction and minimum in the [001] direction, i.e., $T_C^{[111]} > T_C^{[110]} > T_C^{[100]}$. This result is consistent with the present magnetic phase diagram (Fig. 10). The magnetic field angle dependence of $T_C(\theta)$ within the (1$\bar{1}$0) plane is shown in Fig. 14. The solid line is the result of fitting a sine function for each of the two angle ranges, $\theta = 0°$ to 54.7° and $\theta = 54.7°$ to 90°. The fitting curve fits the experimental results quite well. Summarizing the results within the (001) and (1$\bar{1}$0) planes, the T_C curve probably varies smoothly for all field angles, with no discontinuities or anomalies.

IV. DISCUSSION

A. CEF ground state

First, we consider the CEF ground state based on the magnetic anisotropy of the magnetization in the paramagnetic state (Figs. 4 and 5). Due to the CEF effect of cubic
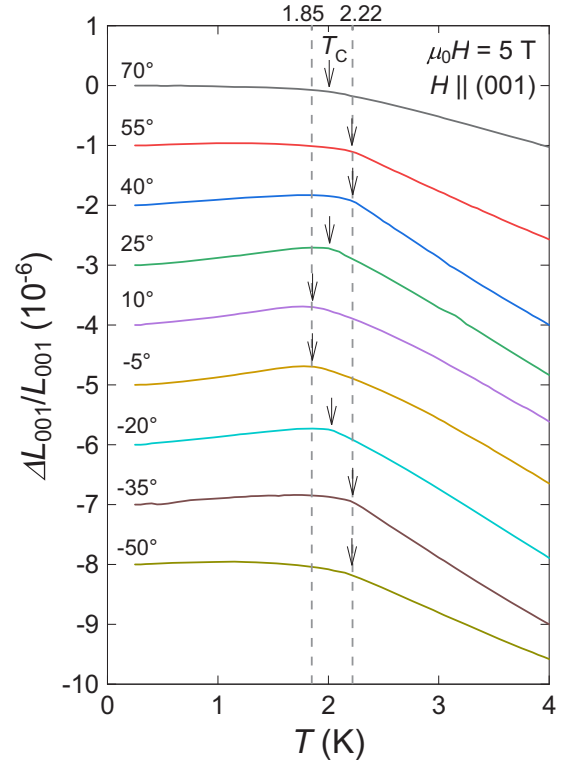
T_h symmetry, the $J = 5/2$ ground-state multiplet in the $4f$ electron of Ce^{3+} splits into a Γ_5 doublet and a Γ_{67} quartet. The wave functions and the magnitudes of the magnetization in the three cubic principal axes for the Γ_5 and Γ_{67} states are summarized in Table I. The magnetization of the Γ_5 doublet is fully isotropic, while that of the Γ_{67} quartet is anisotropic. Taking the ratio of the magnitudes of the magnetization in the three directions in the Γ_{67} quartet, we have $M^{[100]} : M^{[110]} : M^{[111]} = 1.22 : 1.09 : 1$. Surprisingly, this ratio is in good agreement with the experimental values obtained for 2 K and 7 T (see Fig. 4).

We also calculate the temperature and field dependence of magnetization for two CEF schemes based on the CEF model.

TABLE I. Representation, wave functions, and magnitude of the magnetic moment in the three principal axes for Γ_5 and Γ_{67}. The units of the magnetic moment are μ_B/Ce.

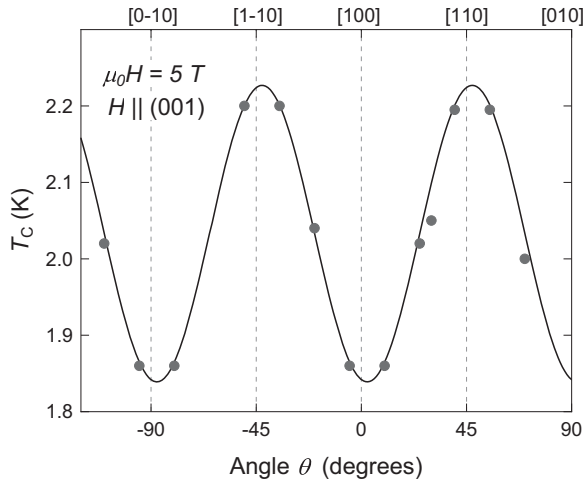| Representation	Wave functions	$M^{[100]}$	$M^{[110]}$	$M^{[111]}$
Γ_5	$\lvert\pm 5/2\rangle$	0.72	0.72	0.72
Γ_{67}	$\lvert\pm 1/2\rangle, \lvert\pm 3/2\rangle$	1.57	1.40	1.29

FIG. 12. Magnetic field angle dependence of the transition temperature $T_C(\theta)$ when a 5 T magnetic field is applied within the (001) plane, obtained from the results of the transverse linear thermal expansion $\Delta L(T)/L$ of CeOs$_4$Sb$_{12}$. The magnetic field angle θ is the angle between the magnetic field direction H and the [100] direction within the (001) plane. In other words, $\theta = 0°$ is the [100] direction, and $\theta = 90°$ is the [010] direction. The solid line is a fit with a single sine function.

We introduce the following Hamiltonian $\mathcal{H}_0$:

$$\mathcal{H}_0 = \mathcal{H}_{CEF} - g_J\mu_B \boldsymbol{J} \cdot \boldsymbol{H}, \tag{1}$$

where $\mathcal{H}_{CEF}$ is the CEF Hamiltonian and the last term is the Zeeman coupling. g_J is the Landé g factor of the $4f$ ground-state multiplet, and $g_J = 6/7$. μ_B is the Bohr magneton. $\mathcal{H}_{CEF}$ in the subspace of the $J = 5/2$ multiplet of Ce^{3+} for T_h symmetry can be expressed as follows:

$$\mathcal{H}_{CEF} = W\frac{O_4^0 + 5O_4^4}{60}, \tag{2}$$

where O_i^j is the Stevens operator and W is the only CEF parameter that determines the magnitude of the CEF energy splitting. The magnetization $\boldsymbol{M}$ is $\boldsymbol{M} = g_J\mu_B\boldsymbol{J}$. The two types of the CEF parameter used in the calculations are listed in Table II. The value of W is chosen so that the energy splitting width of the two CEF levels is 300 K. Figure 15 shows the calculated $M(T)$ curve at 7 T and $M(H)$ curve at 2 K for the two CEF schemes. In the case of the Γ_5 ground state, both $M(T)$ and $M(H)$ data are almost completely isotropic. In the case of the Γ_{67} ground state, on the other hand, magnetic anisotropy is clearly visible at low temperatures and high fields. For both CEF schemes, the calculated magnitudes of the magnetization are more than twice as large as the experimental values. So if we ignore the magnitude of the magnetization, the behavior of

TABLE II. CEF parameter W and CEF energy levels for Γ_5 and Γ_{67} CEF ground states.

W (K)	CEF levels
50	Γ_5 (0 K), Γ_{67} (300 K)
-50	Γ_{67} (0 K), Γ_5 (300 K)

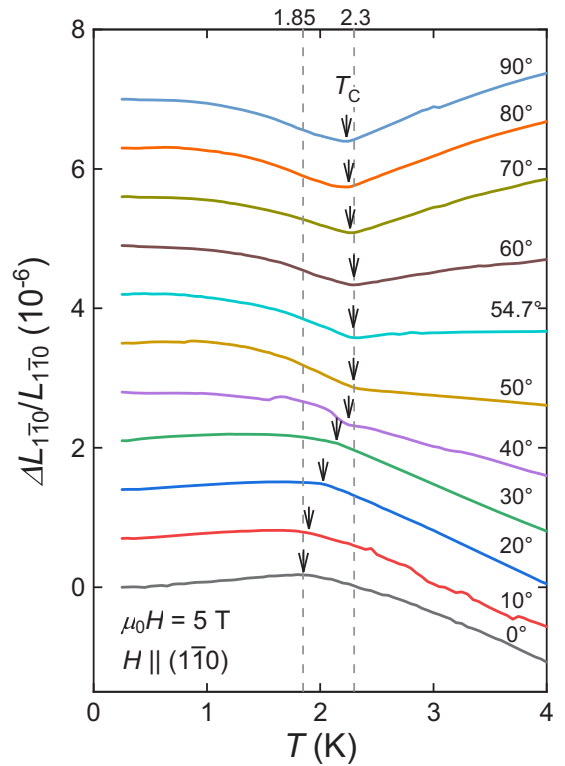FIG. 13. Temperature dependence of the transverse ($H \perp L$) linear thermal expansion $\Delta L(T)/L$ in CeOs$_4$Sb$_{12}$ when a magnetic field of 5 T is applied within the (1$\bar{1}$0) plane. Let θ be the angle between the [001] direction and the direction of the magnetic field within the (1$\bar{1}$0) plane. In other words, $\theta = 0°$ is the [001] direction, $\theta = 54.7°$ is the [111] direction, and $\theta = 90°$ is the [110] direction. The arrows indicate the transition temperature T_C, and the two dashed lines are guides for the eye, corresponding to the maximum and minimum T_C temperatures. The origin of each set of data is shifted so that the data do not overlap.
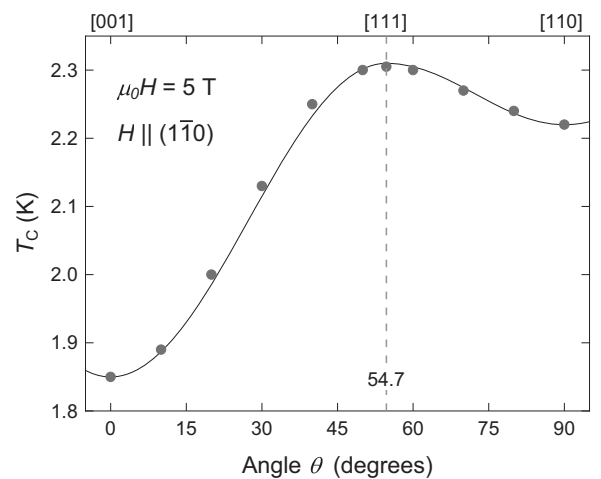

FIG. 14. Magnetic field angle dependence of the transition temperature $T_C(\theta)$ when a magnetic field of 5 T is applied within the (1$\bar{1}$0) plane, obtained from the results of the thermal expansion $\Delta L(T)/L$ in CeOs$_4$Sb$_{12}$. The solid line is the result of fitting a sine function for each of the two angle ranges, $\theta = 0°$ to 54.7° and $\theta = 54.7°$ to 90°.
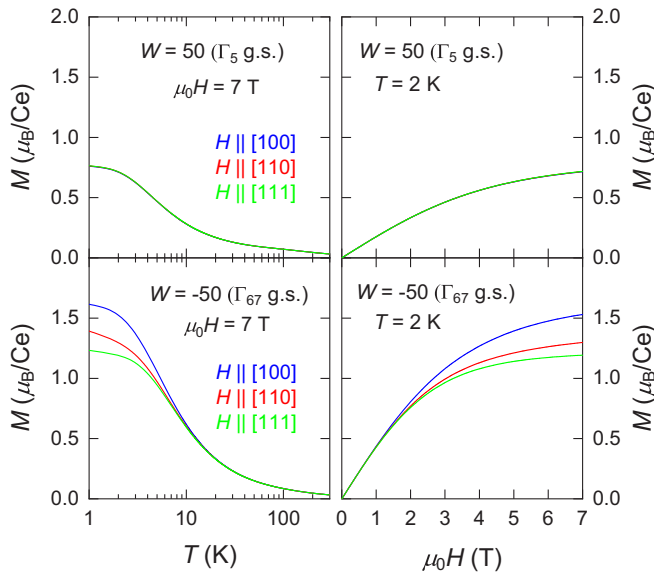
FIG. 15. Calculated $M(T)$ curves at 7 T (left panels) and $M(H)$ curves at 2 K (right panels) for the CEF parameters $W = 50$ (top panels) and $W = -50$ (bottom panels), respectively. These are the results for the three principal axes of the cubic crystal [100], [110], and [111]. Note that the horizontal axis in the $M(T)$ data is a logarithmic scale.

the observed magnetization is clearly more similar to that for the Γ_{67} ground state than for the Γ_5 ground state.

To see how the anisotropy of the magnetization changes when the value of W is changed, the dependence of the values of the magnetization in the three directions on the CEF parameter W at 2 K and 7 T is shown in Fig. 16. For $W > 0$ (with the Γ_5 ground state), as W increases, the magnetic anisotropy decreases, converges to a constant value, and becomes isotropic. For $W < 0$ (with the Γ_{67} ground state), as W decreases, the magnitude of the magnetization gradually decreases and saturates to a constant value, leaving magnetic anisotropy. The magnetic anisotropy for $W > 0$ is just the opposite of the one for $W < 0$. Judging from these calculations, the CEF ground state of CeOs$_4$Sb$_{12}$ is most likely to be the Γ_{67} quartet.

The experimental results of $M(T)$ in Fig. 5 show a small hump around 100 K, while the calculated results show no hump regardless of the value of W. We believe that this hump arises from the c-f hybridization effect. In addition, the remarkably small entropy at low temperatures (the entropy change below T_A is roughly $0.05R \ln 2$ [17]) is probably due to the c-f hybridization effect. Despite the presence of this strong c-f hybridization effect, the magnetic anisotropy of Γ_{67} itself is maintained at low temperatures, suggesting that the c-f hybridization is nearly isotropic. In this respect, the higher-order multipolar moment degrees of freedom of the Γ_{67} quartet may be active even at low temperatures.

According to previous ultrasound experiments, softening in the elastic constants C_{11} and C_{44} has been observed at low temperatures, and it has been reported that the temperature dependence of C_{11} cannot be explained by the CEF ground state of Γ_5 [18]. This is consistent with our result that the CEF ground state is the Γ_{67} quartet. As for the fact that no CEF excited states have been observed in the energy range up to 60 meV in the inelastic neutron scattering experiment [14], the excited state Γ_5 may be more than 60 meV away from the ground state.

CeOs$_4$As$_{12}$ is a Kondo semiconductor with a small hybridization gap, very similar to CeOs$_4$Sb$_{12}$. A clear magnetic anisotropy has been observed in the magnetoresistance of CeOs$_4$As$_{12}$, and it has been reported that the Γ_{67} state is involved in this hybridization gap [19]. This implies that the CEF ground state of CeOs$_4$As$_{12}$ is the Γ_{67} quartet. Therefore the CEF ground states of CeOs$_4$X$_{12}$ with X = P, As, and Sb may all be Γ_{67} quartets, and the magnetic anisotropy of these materials will have to be investigated in more detail.

B. *H-T* phase diagram

Now we will discuss the order parameter of the C phase, assuming that the CEF ground state is the Γ_{67} quartet. The Γ_{67} quartet has degrees of freedom for magnetic dipole, electric quadrupole, and magnetic octupole and thus can produce multiple ordered phases. We can now recall the results for CeB$_6$. This material is a cubic compound (the point-group symmetry at Ce sites is O_h) with a well-isolated Γ_8 quartet (Γ_8 for O_h symmetry and Γ_{67} for T_h symmetry are exactly the same here) in the CEF ground state, which shows AFQ and AFM transitions at $T_Q = 3.3$ K and $T_N = 2.4$ K, respectively. Furthermore, the AFQ phase (so-called phase II) has a field-induced reentrant phase boundary. Hence the AFQ phase of CeB$_6$ is analogous to the C phase of CeOs$_4$Sb$_{12}$. This AFQ phase was clarified more than 20 years ago on the basis of the mean-field approximation theory [20–23]. The AFQ order is of the Γ_5 type, and the octupolar interaction of T_{xyz} plays an important role in the field-induced rise of T_Q.

Here, as for CeB$_6$, we perform numerical calculations for CeOs$_4$Sb$_{12}$ with a two-sublattice model using the mean-field approximation. For more details on the calculation, please refer to Ref. [21]. For sublattice A (or B), we introduce the following effective Hamiltonian $\mathcal{H}^{A(B)}$, which takes into
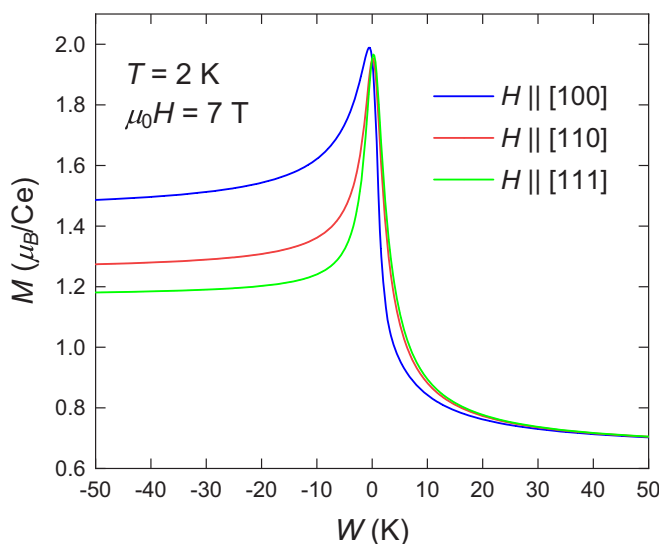

FIG. 16. Dependence of the magnitude of the magnetization M on the CEF parameter W at $T = 2$ K and $\mu_0 H = 7$ T, calculated based on the CEF model.

TABLE III. The values of multipolar interaction parameters used in this calculation, where n is in moles/emu and other values are in degrees Kelvin.

n	$k_{\Gamma3}$	$k_{\Gamma5}$	g_γ	g_α	g_β
-1	-0.055	-0.95	-0.009	-0.009	-0.009

account the three types of multipolar interactions,

$$\mathcal{H}^{\mathrm{A(B)}} = \mathcal{H}_0 + \mathcal{H}_{\mathrm{D}}^{\mathrm{A(B)}} + \mathcal{H}_{\mathrm{Q}}^{\mathrm{A(B)}} + \mathcal{H}_{\mathrm{T}}^{\mathrm{A(B)}}. \quad (3)$$

$\mathcal{H}_{\mathrm{D}}^{\mathrm{A(B)}}$ is the magnetic dipolar interaction Hamiltonian in the molecular field approximation and can be written as

$$\mathcal{H}_{\mathrm{D}}^{\mathrm{A(B)}} = -g_{\mathrm{J}}\mu_{\mathrm{B}}\boldsymbol{J} \cdot (n\langle\boldsymbol{M}\rangle^{\mathrm{B(A)}}), \quad (4)$$

where n is the molecular field coefficient and $\langle X \rangle^{\mathrm{B(A)}}$ represents the thermal average of X in sublattice B (or A). The overall magnetization $\boldsymbol{M}$ can be written using the magnetization $\langle \boldsymbol{M} \rangle^{\mathrm{A}}$ and $\langle \boldsymbol{M} \rangle^{\mathrm{B}}$ for sublattices A and B as follows: $\boldsymbol{M} = \langle \boldsymbol{M} \rangle^{\mathrm{A}} + \langle \boldsymbol{M} \rangle^{\mathrm{B}}$.

Similarly, in the mean-field approximation, the electric quadrupolar interaction Hamiltonian $\mathcal{H}_{\mathrm{Q}}^{\mathrm{A(B)}}$ and the magnetic octupolar interaction Hamiltonian $\mathcal{H}_{\mathrm{T}}^{\mathrm{A(B)}}$ can be written as

$$\mathcal{H}_{\mathrm{Q}}^{\mathrm{A(B)}} = -k_{\Gamma3}\left(\langle O_2^0\rangle^{\mathrm{B(A)}}O_2^0 + \langle O_2^2\rangle^{\mathrm{B(A)}}O_2^2\right)$$
$$- k_{\Gamma5}\left(\langle O_{yz}\rangle^{\mathrm{B(A)}}O_{yz} + \langle O_{zx}\rangle^{\mathrm{B(A)}}O_{zx}\right.$$
$$\left.+ \langle O_{xy}\rangle^{\mathrm{B(A)}}O_{xy}\right), \quad (5)$$

$$\mathcal{H}_{\mathrm{T}}^{\mathrm{A(B)}} = -g_\gamma\langle T_{xyz}\rangle^{\mathrm{B(A)}}T_{xyz} - g_\alpha\left(\langle T_x^\alpha\rangle^{\mathrm{B(A)}}T_x^\alpha + \langle T_y^\alpha\rangle^{\mathrm{B(A)}}T_y^\alpha\right.$$
$$\left.+ \langle T_z^\alpha\rangle^{\mathrm{B(A)}}T_z^\alpha\right) - g_\beta\left(\langle T_x^\beta\rangle^{\mathrm{B(A)}}T_x^\beta + \langle T_y^\beta\rangle^{\mathrm{B(A)}}T_y^\beta\right.$$
$$\left.+ \langle T_z^\beta\rangle^{\mathrm{B(A)}}T_z^\beta\right), \quad (6)$$

where $k_{\Gamma3}$ and $k_{\Gamma5}$ are the molecular field coefficients of the Γ_3-type and Γ_5-type quadrupolar interactions, respectively. g_γ, g_α, and g_β are the molecular field coefficients of the octupolar interaction with Γ_2, Γ_4, and Γ_5 symmetry, respectively. As already reported [22], in the AFQ order of type Γ_5, where all multipolar interactions are antiferro-type interactions and close in strength, the transition temperature increases most significantly with magnetic field. We therefore set the value of $k_{\Gamma5}$ so that the AFQ transition temperature is 1 K at zero field. The other interaction coefficients are chosen to be slightly weaker than the Γ_5-type quadrupolar interaction. The values of the parameters obtained in this way are summarized in Table III.

Figure 17 shows the magnetic phase diagram obtained from the present calculation. The AFQ order parameter in zero field is the linear combination of the components O_{xy}, O_{yz}, and O_{zx} of the Γ_5-type quadrupolar moment. When a magnetic field is applied, various staggered moments are induced depending on the direction of the field. Table IV summarizes the staggered moments induced by the application of magnetic fields along the three principal axes. It is important to note that the staggered octupolar moment of T_{xyz} is induced in all directions. The energy gain of this antiferro-octupolar interaction increases significantly with the magnetic field, which leads to
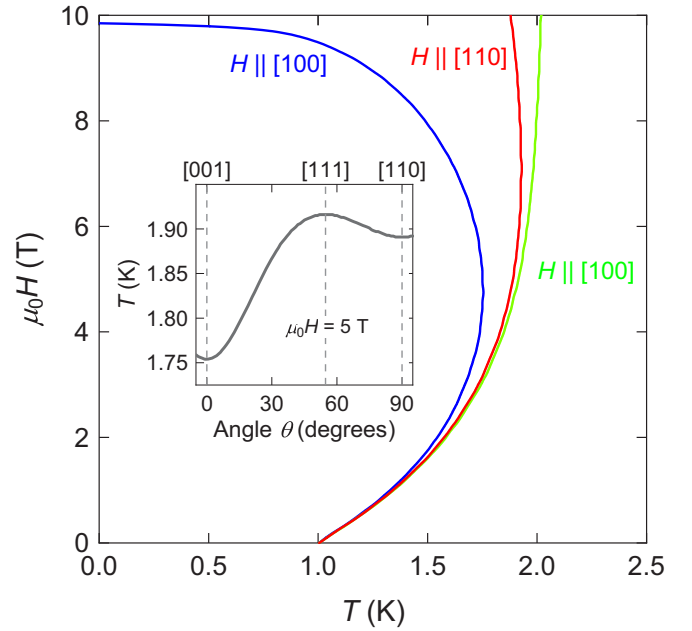

FIG. 17. Magnetic phase diagram of the cubic crystal for the three principal axes obtained from the present numerical calculations. The inset shows the magnetic field direction dependence of the AFQ transition temperature T_{Q} within the $(1\bar{1}0)$ plane at a magnetic field of 5 T. $\theta = 0°$ is the [001] direction, and $\theta = 90°$ is the [110] direction.

a large increase in T_{Q}. The value of $T_{\mathrm{Q}}(H)$ in magnetic fields is highest in the [111] direction and lowest in the [100] direction. The maximum value of $T_{\mathrm{Q}}(H)$ for $H \parallel$ [111] is more than twice the value at zero field, in good agreement with the experimental results. In addition, the value of $T_{\mathrm{Q}}(H)$ for $H \parallel$ [100] goes to zero faster than for the other magnetic field directions. This behavior has indeed been confirmed experimentally (see Fig. 1) [7].

The inset of Fig. 17 shows the calculated field direction dependence of T_{Q} at 5 T within the $(1\bar{1}0)$ plane. The $T_{\mathrm{Q}}(\theta)$ curve shows a smooth variation with respect to the magnetic field angle θ and is in almost quantitatively good agreement with the experimental results (see Fig. 14). This behavior can be interpreted as the proportions of the order parameters O_{xy}, O_{yz}, and O_{zx} varying continuously with the direction of the magnetic field. It should be emphasized that in the absence of Γ_5-type quadrupolar interaction or Γ_2-type octupolar interaction, the transition temperature is hardly increased by the magnetic field. Figure 18 shows the temperature varia-

TABLE IV. Order parameters and field-induced staggered moments for the three principal axes of the cubic crystal in the Γ_5-type AFQ phase.

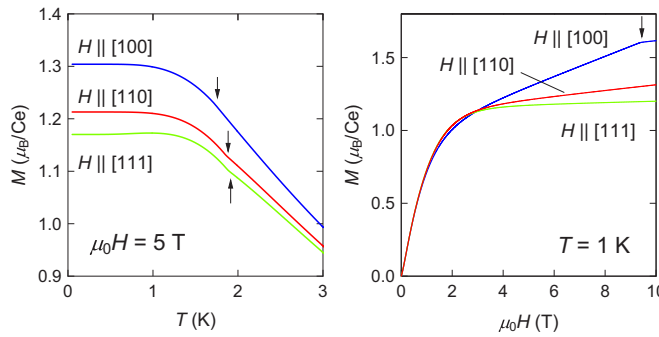| Field	Order parameter	Induced staggered moments
[001]	O_{xy}	T_{xyz}
[110]	$O_{yz} + O_{zx}$	J_z, T_{xyz}, T_z^α
[111]	$O_{yz} + O_{zx} + O_{xy}$	$J_x + J_y + J_z,$
		$T_{xyz}, T_x^\alpha + T_y^\alpha + T_z^\alpha$

FIG. 18. Temperature dependence of the magnetization $M(T)$ at 5 T (left panel) and the magnetization $M(H)$ process at 1 K (right panel) in the Γ_5-type AFQ model. Arrows indicate the C-phase transition point.

tion of the magnetization $M(T)$ at 5 T (left panel) and the calculated isothermal magnetization $M(H)$ process at 1 K (right panel). The phase transition points are indicated by arrows. It is noteworthy that the magnetization anomaly at T_Q is very weak in the $M(T)$ data at 5 T. In particular, the anomaly at $H \parallel [100]$ is not noticeable at all. This feature is consistent with the experimental results (see Fig. 1). The $M(H)$ curve at 1 K is isotropic up to around 3 T, but magnetic anisotropy develops at higher fields. This result is somewhat similar to the experimental result of the $M(H)$ curve at 0.3 K (Fig. 2), although the comparison is not simple due to the presence of AFM order at low fields in the experimental results.

Returning to Table IV, the characteristic feature for $H \parallel [001]$ in phase C is that the staggered moment of the magnetic dipole is not induced. This is consistent with the results of elastic neutron scattering experiments, where only ferromagnetic components are observed in the C phase [16]. The weak anomaly in the $M(T)$ data of $H \parallel [100]$ at T_Q (Fig. 1) can be attributed to the absence of the staggered moment of the magnetic dipole. Therefore the 4f electron at low temperatures should not be a localized picture, but strangely enough, many features of the C phase can be well reproduced by the Γ_5-type AFQ order.

Finally, we discuss the results of thermal expansion in phase B. If the Γ_5-type AFQ order is realized in the B and C phases, the symmetry of the crystal lattice should decrease from cubic in both phases. The experimental results show that in phase B, the magnetization (Fig. 1) is isotropic, but the thermal expansion (Fig. 6) is anisotropic. Therefore the observed anisotropy of thermal expansion below T_B might provide further evidence for Γ_5-type AFQ ordering in phase B.

The magnetic phase diagram of $CeOs_4Sb_{12}$ at low field is more similar to that of $Ce_{0.75}La_{0.25}B_6$ than that of CeB_6. $Ce_{0.75}La_{0.25}B_6$ has four phases, phases I, II, III, and IV: Phase I is the paramagnetic phase, phase II is the AFQ-ordered phase of the Γ_5 type, phase III is the coexistence of AF and AFQ ordering, and phase IV is the antiferro-octupolar order of T^β [24]. In zero field, the second-order transition to phase IV and the first-order transition to phase III occur at 1.65 and 1.1 K, respectively. If the A, B, and C

phases of $CeOs_4Sb_{12}$ correspond to phases IV, III, and II of $Ce_{0.75}La_{0.25}B_6$, T_B should be a first-order transition. In this experiment, however, there is no sign of a first-order transition at T_B. On the other hand, in nuclear quadrupole resonance (NQR) experiments [10], temperature hysteresis was observed at low temperatures around T_B, so there is still a possibility that T_B is a first-order transition. The magnetization in phase IV is isotropic, while the magnetization in phase III is anisotropic. In contrast, in $CeOs_4Sb_{12}$, the magnetization is isotropic in both phases A and B. Thus the low-field ordered phases of $CeOs_4Sb_{12}$ are qualitatively different from those of $Ce_{0.75}La_{0.25}B_6$ and may have a different multipole order.

Recently, the Ce-based Kondo semiconductor $Ce(Ru, Os)_2Al_{10}$ has also attracted much attention. The crystal structure of this material is orthorhombic, and the CEF ground state is a Kramers doublet. It shows an AFM transition at a relatively high temperature of about 30 K, despite the small ordered moment. The high AFM transition temperature is likely to be associated with the strong anisotropic c-f hybridization effect in this material [25,26]. Thus $CeOs_4Sb_{12}$ and $Ce(Ru, Os)_2Al_{10}$ are Kondo semiconductors with strong c-f hybridization effects and exhibit somewhat unexpected phase transitions. In this respect, further studies of the phase transition in a Ce-based Kondo semiconductor will be valuable in understanding the nature of the c-f hybridization effect.

V. SUMMARY

In conclusion, we have performed dc magnetization, thermal expansion, and magnetostriction measurements on a single-crystal sample of $CeOs_4Sb_{12}$ to investigate the three ordered phases A, B, and C and the ground state of the CEF levels. A magnetic phase diagram for the three principal axes of the cubic crystal is obtained, and the magnetic anisotropy of the transition temperature T_C to the C phase is $T_C^{[111]} > T_C^{[110]} > T_C^{[100]}$. Comparing the magnetic anisotropy of the magnetization at low temperatures with the calculations in the CEF model, we found that the CEF ground state is most likely the magnetically anisotropic Γ_{67} quartet, contrary to previous reports that the CEF ground state is the magnetically isotropic Γ_5 doublet. We also performed numerical calculations using the mean-field approximation under the assumption of the Γ_{67} CEF ground state. The observed magnetic phase diagram of phase C is in good agreement with the magnetic phase diagram calculated for the Γ_5-type AFQ order. The large enhancement of the transition temperature T_C by the application of an external magnetic field can be explained by the Γ_2-type antiferro-octupolar interaction. Due to the strong c-f hybridization effect, the entropy and the magnitude of the magnetic moment of the Γ_{67} quartet are largely lost at low temperatures. Nevertheless, the magnetic anisotropy of the Γ_{67} quartet is maintained at low temperatures, suggesting that the c-f hybridization effect is nearly isotropic. This isotropic c-f hybridization effect is thought to play an important role in the occurrence of the unusual AFQ order. Since the higher-order multipolar moments of the Γ_{67} quartet are probably activated at low temperatures, new multipole orders may emerge by applying pressure or substituting elements.

$CeOs_4Sb_{12}$ has also been suggested as a possible topological insulator based on band theory calculations [27], making it a unique material that could be the setting for new research involving higher-order multipolar moments and topological insulators.

[1] E. D. Bauer, A. Slebarski, E. J. Freeman, C. Sirvent, and M. B. Maple, J. Phys.: Condens. Matter **13**, 4495 (2001).

[2] X. Lou, T. L. Yu, Y. H. Song, C. H. P. Wen, W. Z. Wei, A. Leithe-Jasper, Z. F. Ding, L. Shu, S. Kirchner, H. C. Xu, R. Peng, and D. L. Feng, Phys. Rev. Lett. **126**, 136402 (2021).

[3] H. Harima and K. Takegahara, J. Phys.: Condens. Matter **15**, S2081 (2003).

[4] Y. Imai, K. Sakurazawa, and T. Saso, J. Phys. Soc. Jpn. **75**, 33706 (2006).

[5] Y. Imai, K. Sakurazawa, and T. Saso, J. Magn. Magn. Mater. **310**, 243 (2007).

[6] M. Matsunami, R. Eguchi, T. Kiss, K. Horiba, A. Chainani, M. Taguchi, K. Yamamoto, T. Togashi, S. Watanabe, X. Y. Wang, C. T. Chen, Y. Senba, H. Ohashi, H. Sugawara, H. Sato, H. Harima, and S. Shin, Phys. Rev. Lett. **102**, 036403 (2009).

[7] H. Sugawara, S. Osaki, M. Kobayashi, T. Namiki, S. R. Saha, Y. Aoki, and H. Sato, Phys. Rev. B **71**, 125127 (2005).

[8] P. C. Ho, J. Singleton, P. A. Goddard, F. F. Balakirev, S. Chikara, T. Yanagisawa, M. B. Maple, D. B. Shrekenhamer, X. Lee, and A. T. Thomas, Phys. Rev. B **94**, 205140 (2016).

[9] M. Yogi, H. Kotegawa, G. Q. Zheng, Y. Kitaoka, S. Osaki, H. Sugawara, and H. Sato, J. Magn. Magn. Mater. **272**, E45 (2004).

[10] M. Yogi, H. Kotegawa, G. Q. Zhang, Y. Kitaoka, S. Ohsaki, H. Sugawara, and H. Sato, J. Phys. Soc. Jpn. **74**, 1950 (2005).

[11] K. Iwasa, S. Itobe, C. P. Yang, Y. Murakami, M. Kohgi, K. Kuwahara, H. Sugawara, H. Sato, N. Aso, T. Tayama, and T. Sakakibara, J. Phys. Soc. Jpn. **77**, 318 (2008).

[12] M. Yogi, H. Niki, M. Yashima, H. Mukuda, Y. Kitaoka, H. Sugawara, and H. Sato, J. Phys. Soc. Jpn. **78**, 53703 (2009).

[13] T. Tayama, W. Ohmachi, M. Wansawa, D. Yutani, T. Sakakibara, H. Sugawara, and H. Sato, J. Phys. Soc. Jpn. **84**, 104701 (2015).

[14] C. P. Yang, H. Wang, K. Iwasa, M. Kohgi, H. Sugawara, and H. Sato, Appl. Phys. Lett. **89**, 82508 (2006).

[15] C. P. Yang, H. Wang, J. F. Hu, K. Iwasa, M. Kohgi, H. Sugawara, and H. Sato, J. Phys. Chem. C **111**, 2391 (2007).

[16] K. Iwasa, C. P. Yang, M. Kohgi, H. Sugawara, H. Sato, and N. Aso, J. Magn. Magn. Mater. **310**, 268 (2007).

[17] T. Namiki, Y. Aoki, H. Sugawara, and H. Sato, Acta Phys. Pol. B **34**, 1161 (2003).

[18] Y. Nakanishi, T. Kumagai, M. Oikawa, T. Tanizawa, M. Yoshizawa, H. Sugawara, and H. Sato, Phys. Rev. B **75**, 134411 (2007).

[19] T. Cichorek, L. Bochenek, R. Wawryk, and Z. Henkie, Phys. Status Solidi B **250**, 646 (2013).

[20] R. Shiina, H. Shiba, and P. Thalmeier, J. Phys. Soc. Jpn. **66**, 1741 (1997).

[21] O. Sakai, R. Shiina, H. Shiba, and P. Thalmeier, J. Phys. Soc. Jpn. **66**, 3005 (1997).

[22] R. Shiina, H. Shiba, and P. Thalmeier, J. Magn. Magn. Mater. **177**, 303 (1998).

[23] H. Shiba, O. Sakai, and R. Shiina, J. Phys. Soc. Jpn. **68**, 1988 (1999).

[24] T. Tayama, T. Sakakibara, K. Tenya, H. Amitsuka, and S. Kunii, J. Phys. Soc. Jpn. **66**, 2268 (1997).

[25] S.-i. Kimura, T. Iizuka, H. Miyazaki, A. Irizawa, Y. Muro, and T. Takabatake, Phys. Rev. Lett. **106**, 056404 (2011).

[26] S.-i. Kimura, H. Tanida, M. Sera, Y. Muro, T. Takabatake, T. Nishioka, M. Matsumura, and R. Kobayashi, Phys. Rev. B **91**, 241120(R) (2015).

[27] B. H. Yan, L. Muchler, X. L. Qi, S. C. Zhang, and C. Felser, Phys. Rev. B **85**, 165125 (2012).